AIP Publishing Applied Physics Letters ACCEPTED MANUSCRIPT
This is the author's peer reviewed, accepted manuscript. However, the online version of record will be different from this version once it has been copyedited and typeset.
PLEASE CITE THIS ARTICLE AS DOI: 10.1063/5.0107667

Continuous wave operation of terahertz metasurface quantum-cascade VECSEL with a long intra-cryostat cavity

Yu Wu,[1, a)] Christopher A. Curwen,[2] Darren J. Hayton,[2] John L. Reno,[3] Benjamin S. Williams[1]
[1]*Department of Electrical and Computer Engineering, University of California, Los Angeles, California 90095, USA*
[2]*Jet Propulsion Laboratory, California Institute of Technology, Pasadena, California 91109, USA*
[3]*Sandia National Laboratories, Center of Integrated Nanotechnologies, MS 1303, Albuquerque, New Mexico 87185, USA*
a) Authors to whom correspondence should be addressed: ywu17@ucla.edu

ABSTRACT

We report continuous wave (cw) operation of a terahertz quantum-cascade vertical-external-cavity surface-emitting laser (QC-VECSEL) with external cavity length of approximately 30 mm, benefited by an intra-cryostat focusing cavity. Compared to previous plano-plano cavities, an off-axis paraboloid mirror is introduced into the external cavity as a focusing element to reduce the diffraction loss and enable cw lasing using small-area metasurfaces and long cavity lengths. The device shows lasing operation in cw mode up to 111 K, and cw output power up to 11.5 mW at 77 K (0.5% wall-plug efficiency). A circular, directive beam pattern is collected, and free-running linewidths on the order of tens of kHz are measured over tens of seconds.

The terahertz (THz) quantum-cascade (QC) vertical-external-cavity surface-emitting laser (VECSEL) has been demonstrated as a solid-state source of high-power, coherent terahertz radiation which exhibits a high-quality beam pattern.[1–3] Its key component is a metasurface loaded with QC-gain material that acts as an amplifying reflector and is paired with a partially transmissive output coupler to form a laser cavity. Previously, we have shown the benefit of short cavities with wavelength-scale lengths; such cavities exhibit a large free-spectral-range (FSR), and by changing the external cavity length, over 20% continuous tuning of a single lasing mode has been observed.[4] So far, the demonstrations of QC-VECSELs have been limited to simple plano-plano cavities using flat optics. This is most straightforward since spherical output coupler mirrors are not readily available in THz frequency range. Also, cryogenic operation temperatures are required for THz QC-lasers, and to avoid excess atmospheric losses and etalon effects from a cryostat window the external cavity should be built entirely within the cryostat. However, due to increasing diffraction loss, the maximum plano-plano cavity lengths have been limited to ~10 mm, and this was only achieved by using a metasurface with a large central circular bias area of diameter 2.4 mm.[5] Such a metasurface consumes large electrical power, which prevents continuous wave (cw) operation. Nonetheless, there are many circumstances which would necessitate a longer cavity, for example, insertion of additional optical elements (e.g. for Littrow cavity tuning), increasing the round-trip photon time for the study of mode-locking operation in QC-lasers, reducing the FSR to encourage broadband multi-mode lasing, or increasing the cavity quality factor. While a planar focusing QC-metasurface can be used to help stabilize the cavity mode, such an approach results in a large spot on the metasurface and a small spot on the output coupler, still requiring a large metasurface device. Also, current designs are based upon resonant metasurface elements, and thus are not suitable for broadband applications.[6]

In this Letter, we introduce an off-axis paraboloid (OAP) mirror into the VECSEL cavity to reduce the intra-cavity diffraction loss and allow cw lasing for 30-mm cavity lengths. The cavity mounted inside the cryostat is shown in Fig. 1(a), it consists of an OAP mirror with a focal length of 12.7 mm, a planar quartz output coupler deposited with inductive-mesh and an active QC-metasurface. The metasurface used in the following numerical simulation and experimental demonstration is depicted in Fig. 1(b). It is spatially uniform across the 1.5×1.5 mm^2 area, while electrical bias is selectively applied to a small central circular area of diameter $d = 0.4$ mm for reduced injection current. The array of metal-metal ridge antennas is designed with a ridge width of 12.2 μm and period

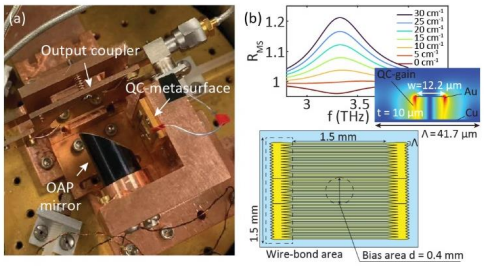

FIG. 1. (a) Top view of the cavity in the cryostat. (b) The lower figure is a top-down schematic of the active QC-metasurface used in this paper with a central bias diameter of 0.4 mm. The inset points out the dimension and E-field distribution at resonance frequency of a single ridge antenna. The upper figure shows FEM simulated active metasurface reflectance with respect to various uniform ISB gain.

AIP Publishing Applied Physics Letters ACCEPTED MANUSCRIPT
This is the author's peer reviewed, accepted manuscript. However, the online version of record will be different from this version once it has been copyedited and typeset.
PLEASE CITE THIS ARTICLE AS DOI: 10.1063/5.0107667

of 41.7 μm, similar as that in Ref. 4. Its amplification factor is characterized using full-wave 2D finite-element (FEM) electromagnetic reflectance simulation (Ansys HFSS). In the FEM simulation, the metasurface is assumed to be infinite in extent, where a single metasurface period is simulated with periodic boundary conditions. Simulated losses in the metal thin films are estimated using the Drude model ($n_{Au} = 5.9 \times 10^{22}$ cm^{-3}, $\tau_{Au,77\,K} =$ 39 fs [7]), while the semiconductor layer is modeled to have a frequency-independent intersubband (ISB) gain for simplicity. The simulated active reflectance R_{MS} of this metasurface indicates a resonance frequency near 3.3 THz with quality factor $Q \approx 7$ and a transparency gain coefficient of $g_{tr} = 5.2$ cm^{-1}. The transparency gain is obtained through numerical fitting of R_{MS} with respect to ISB gain coefficient g according to [2]:

$$R_{MS} = e^{\xi(\nu)(g-g_{tr})}, \quad (1)$$

where $\xi(\nu)$ is an effective interaction length which contains the metasurface spectral response with a peak value of $\xi_0 =$ 0.0077 cm at resonance frequency.

To quantify the intra-cavity diffraction loss in VECSEL cavities, we constructed a 2D full-wave electromagnetic external cavity model using COMSOL Multiphysics (Fig. 2). It accounts for the finite dimension of the metasurface along one axis, which contains 35 periods of ridge antennas where only the central 9 antennas are selectively biased and loaded with uniform QC-gain. The same metal losses are applied as in the reflectance simulation. For simplicity, the output coupler is modeled as a perfect electric conductor (PEC) boundary to form an external cavity with adjustable cavity lengths. The threshold QC-gain coefficient g_{th} is that needed to make the cavity eigenfrequency fully real (i.e. no net loss or gain). In Fig. 2(a), the QC-gain coefficient needed to compensate for overall losses in plano-plano cavities are plotted as a function of external cavity length ranging from 0.5 mm to 8 mm. As expected, g_{th} increases dramatically with respect to L_c and exceeds 100 cm^{-1} for a cavity length of 8 mm, indicating that lasing is prohibited in such a VECSEL cavity (blue curve). This trend actually describes two entangled "diffractive" effects: (1) the general increase in the cavity eigenmode spot size that increases its overlap with the unbiased area of the metasurface,[2] and (2) scattering losses out of the cavity eigenmode. By enlarging the bias area to $d =$ 0.7 mm, i.e. selectively adding gain to the central 17 antennas, g_{th} as well as round-trip losses are reduced with slower increase with respect to L_c (red curve). However, more current draw and heat dissipation are required as a tradeoff. As a comparison, we introduce a curved PEC facet as an OAP mirror into the simulation model and center the biased area at its focal point (Fig. 2(d)). The threshold gain coefficient is then reduced to a reasonable value of $g_{th} =$ 6.5 cm^{-1} for a cavity length around 18.7 mm, a value smaller than any plano-plano cavities results and close to the transparency gain of the active metasurface. This is equivalent to excess loss of 1% per round trip in this 2D model – an actual 3D cavity would exhibit twice that. Furthermore, it is worth noting that these values are highly dependent upon the absorbance in the unbiased region of the metasurface. For example, in our FEM simulations we assume only metal losses are loaded in the unbiased antennas (to be active region "agnostic"). However, in a real case, there may exist strong absorption loss coming from intersubband resonance within the active material,[8] which will exacerbate the round-trip losses in a plano-plano cavity.

The metasurface is loaded with a GaAs/$Al_{0.15}Ga_{0.85}$As QC-active region grown 10-μm thick by molecular beam epitaxy (wafer VB0739). It is based upon the hybrid bound-to-continuum/resonant-phonon design scheme and exhibits over 1 THz gain bandwidth peaking at 3.4 THz. The same wafer has been used in Refs. 4,9,10, and the characterization of metal-metal waveguide QC-laser based on this wafer can

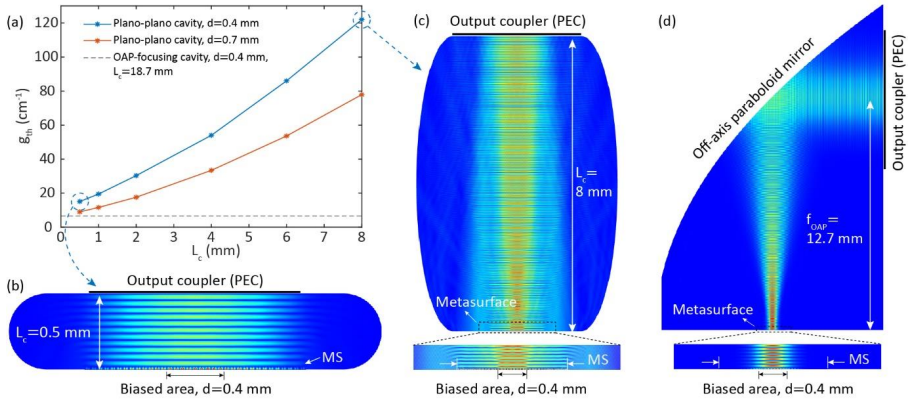

FIG. 2. (a) Simulated threshold gain coefficients with respect to external cavity lengths in plano-plano cavities. In the FEM simulation, 35 ridge antennas (see Fig. 1(b)) are modeled with a total length around 1.5 mm, while only the central 9 (blue curve) or 17 (red curve) antennas are selectively biased, corresponding to a bias diameter of 0.4 mm or 0.7 mm. (b-c) E-field plots of FEM simulated plano-plano cavities with cavity length of 0.5 mm and 8 mm, in the case of using a 0.4 mm bias diameter metasurface. The absorbing boundaries will collect the diffracted light which is considered as the intra-cavity diffraction loss. (d) E-field plot of FEM simulated OAP-focusing cavity with a cavity length of 18.7 mm and bias diameter of 0.4 mm, which clearly shows the improvement in light diffraction. The value of g_{th} in this case is pointed out by the black dashed line in (a) for better comparison.

AIP Publishing Applied Physics Letters ACCEPTED MANUSCRIPT
This is the author's peer reviewed, accepted manuscript. However, the online version of record will be different from this version once it has been copyedited and typeset.
PLEASE CITE THIS ARTICLE AS DOI: 10.1063/5.0107667

be found in the supplementary material in Ref. 9. Microfabrication of the wafer into metasurfaces took place in the standard metal-metal waveguide process, using a Cu-Cu thermocompression wafer bonding technique.[11] The metasurface was placed in the OAP-focusing cavity with length ~30 mm (shown in Fig. 1(a)) paired with an output coupler of reflectance $R_{OC} \approx 95\%$. Alignment of the output coupler takes place at room-temperature via alignment screws on the output mount with the aid of a He:Ne laser; alignment is preserved following cooldown within a liquid-nitrogen cooled vacuum cryostat. The resulting QC-VECSEL has been experimentally characterized both in pulsed mode with 0.5% duty cycle (500 ns pulses at 10 kHz repetition rate) and in cw mode. The power and voltage vs. current (*P-I-V*) curves are plotted in Fig. 3 at various temperatures. The output power was collected using a pyroelectric detector (GentecEO) and is measured as 20 mW and 11.5 mW at 77 K, with a peak wall-plug efficiency of 0.8% and 0.5%, a slope efficiency of 313 mW/A and 272 mW/A in pulsed and cw mode respectively. The reported power has been corrected based on 65% transmittance of the 3 mm thick polyethylene cryostat window. *P-I* characteristics as a function of varying heat-sink temperatures (*T*) demonstrate that the device lases up to a maximum temperature of 132 K in pulsed mode and 105 K in cw mode. The insets of Fig. 3 show the phenomenological fit to the expression $J_{th} = J_0 \exp(T/T_0)$, which results in values of $T_{0,\,pulsed} = 145$ K and $T_{0,\,cw} = 88$ K. By using a more reflective output coupler ($R_{OC} > 99\%$), the maximum operation temperatures increase to 145 K in pulsed mode and 111 K in cw mode, at a sacrifice of lower output power (see Supplementary Section S2). As a comparison, the maximum pulsed-mode operating temperature demonstrated using the same QC-wafer (VB0739) has been measured to be 170 K in a metal–metal ridge waveguide and 129 K for a focusing metasurface VECSEL with $L_c = 2.1$ mm.[9] The improved temperature performance of a QC-VECSEL based on OAP-focusing cavity design is a clear indication that while it still has larger total loss compared with the ridge waveguide, the OAP-focusing cavity has less loss and improved beam spot confinement in the biased area compared with VECSELs with more than 10× shorter cavities.

The emission spectra were collected using a Fourier-transform infrared spectrometer (FTIR, Nicolet 8700) and are plotted in Fig. 4 (a-b) for pulsed and cw mode respectively. In cw mode, a single lasing peak is observed around 3.37 THz despite the fact that the gain bandwidth of the metasurface is at least 100 times larger than the FSR (5 GHz). This single mode operation is primarily due to the lack of spatial hole burning in QC-VECSELs, as all the longitudinal modes supported in the external cavity interact with the QC-gain material through the same metasurface resonance with nearly the same spatial overlap.[5] In contrast, the FTIR spectra in pulsed mode show lasing bandwidth around 58 GHz. Though we are not able to spectrally resolve individual modes due to the limited FTIR resolution of 7.5 GHz, it indicates multi-mode lasing operation of ~10 modes. This multi-mode lasing is still present for pulse-widths of at least up to 500 μs, which indicates that the collapse to single-mode

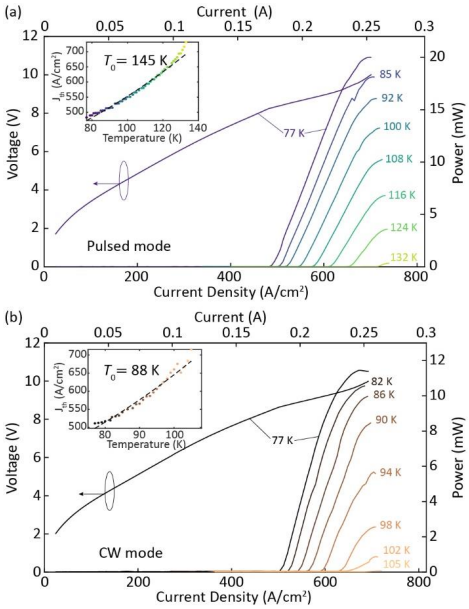

FIG. 3. Pulsed (a) and cw (b) *P-I-V* characteristics of the QC-VECSEL using an output coupler with $R_{OC} \approx 95\%$. *I-V* curves are measured at 77 K while *P-I* curves are collected as a function of varying heat-sink temperature *T*. Insets show a threshold current density vs heat-sink temperature.

operation takes place on relatively long millisecond timescales. The inset plot shows a circular, Gaussian far-field beam profile obtained in pulsed mode, which implies lasing occurs in a single transverse mode.

Next, we performed high-resolution spectral measurements by downconverting the cw QC-VECSEL emission into the RF using a sub-harmonic Schottky-diode mixer pumped by the 35th harmonic of a 100 GHz local oscillator (LO). The beatnote signal at f_{BN} was measured using a spectrum analyzer (Keysight N9020a) with a resolution bandwidth of 180 Hz, which allowed for characterization of the free-running linewidth and electrical tuning of the laser emission (Fig. 4(c), the beatnote center frequencies are subtracted for clarity). As we increased the LO frequency, f_{BN} increased accordingly, which indicates that the lasing frequency is smaller than LO frequency, i.e. $mf_{LO} - f_{THz} = f_{BN}$. Based on an accurate beatnote frequency, we obtain the exact lasing frequency at 3.3774678 THz. Free-running linewidths are obtained by operating the spectrum analyzer in the Max Hold mode over 10 seconds; the measured values are in the range of 20 – 50 kHz. This value is considerably smaller than the free-running linewidths of waveguide-based THz QC-lasers, which are typically on the order of a few MHz when measured over times of more than a few seconds, and are primarily limited by temperature and current fluctuations.[12–15] This is expected, since in a QC-VECSEL most of the cavity mode resides within vacuum and not the QC-active material,

AIP Publishing Applied Physics Letters ACCEPTED MANUSCRIPT
This is the author's peer reviewed, accepted manuscript. However, the online version of record will be different from this version once it has been copyedited and typeset.
PLEASE CITE THIS ARTICLE AS DOI: 10.1063/5.0107667

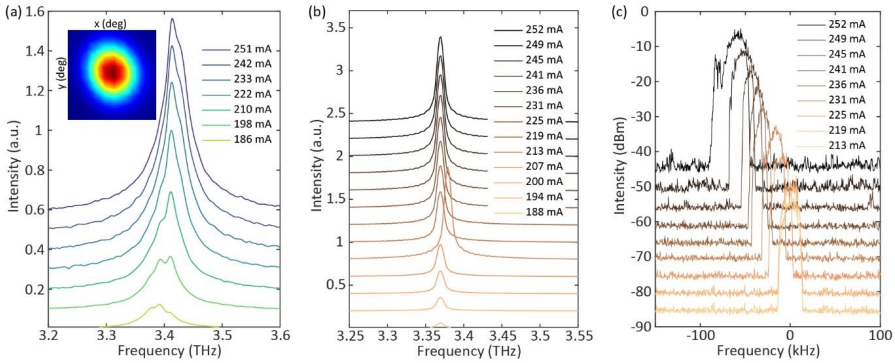

FIG. 4. Pulsed (a) and cw (b) lasing spectra measured as a function of applied bias current at 77 K. The inset of (a) shows a high quality far-field beam pattern. It was measured using a two-axis scanning pyroelectric detector with a 2-mm-diameter aperture rotating at a constant distance of ~15 cm from the device. (c) Free-running beatnotes measured in cw mode as a function of applied bias current. It was obtained by operating the spectrum analyzer (Keysight N9020a) in the Max. Hold mode over 10 seconds with a resolution bandwidth as small as 180 Hz.

and hence is less sensitive to refractive index fluctuations of the semiconductor. This is consistent with the fact that the tuning coefficient is measured to be 1.7 kHz/mA, which is 3-4 orders of magnitude smaller than that reported for waveguide-based QC-lasers, or even short-cavity VECSELs. We also note that the free-running Max Hold linewidth is considerably smaller than the value of ~20 MHz measured in a ~0.5-mm long plano-plano cavity VECSEL,[16] in which mechanical vibrations originating from the output coupler mount are believed to dominate. This is expected, as the frequency sensitivity to output coupler vibrations scales inversely with cavity length ($\delta\nu/\nu = \delta L_c/L_c$).

In conclusion, we introduce an intra-cryostat OAP-focusing cavity design for QC-VECSELs, which enables cw operation at 77 K in an external cavity length ~30 mm. This is the longest cavity length reported to date with the FSR easily accessible for beatnote measurement and injection locking using modest RF instrumentation.[17,18] It is notable that there is no evidence of spontaneous frequency comb operation in QC-VECSELs as that has been demonstrated in ridge waveguide QC-lasers[19,20] or ring cavity QC-lasers[21,22] – this may be related to the lack of spatial hole burning within the metasurface, or the fact that no effort towards dispersion compensation has been attempted yet. Nonetheless, we consider this cavity design as an excellent platform to study THz QC-VECSEL based frequency combs through RF modulation of the QC-gain.[23,24] Aside from the additional functionality, excellent performance has been demonstrated in this device, such as a high output power, low current consumption, low divergence beam pattern, and narrow free-running linewidth. Maximum operating temperatures in both pulsed and cw are better than observed in QC-VECSELs with the same active region but using plano-plano cavities with much larger bias diameters.[9] High frequency stability in QC-lasers is mandatory for applications in astronomical and atmospheric high-resolution spectroscopy of narrow molecule absorption lines.[25,26] Free-running linewidths on the order of tens of kHz demonstrated in this paper provides a good starting point for further stabilization using method such as frequency locking to gas absorption lines[27] or high-finesse optical cavities,[28] and phase-locking to optical frequency combs[29] or harmonics of a microwave frequency standard.[13] However, this comes at the expense of a limited electrical frequency tuning range; future work will be required to combine this approach with frequency agility.

Supplementary Material

See supplementary material for data on output coupler transmittance, temperature performance with a more reflective output coupler, and discussion on OAP-focusing cavity alignment tolerance.

Acknowledgments

Microfabrication was performed at the UCLA Nanoelectronics Research Facility, wire bonding was performed at the UCLA Center for High Frequency Electronics, and high-resolution spectral measurements were performed at NASA Jet Propulsion Laboratory. This work was performed, in part, at the Center for Integrated Nanotechnologies, an Office of Science User Facility operated for the U.S. Department of Energy (DOE) Office of Science. Sandia National Laboratories is a multimission laboratory managed and operated by National Technology and Engineering Solution of Sandia, LLC., a wholly owned subsidiary of Honeywell International, Inc., for the U.S. Department of Energy's National Nuclear Security Administration under contract DE-NA-0003525. Partial funding was provided by the National Science Foundation (2041165), and the National Aeronautics and Space Administration (80NSSC19K0700).

Data Availability

The data that supports the findings of this study are available within the article and its supplementary material.

AIP Publishing Applied Physics Letters ACCEPTED MANUSCRIPT
This is the author's peer reviewed, accepted manuscript. However, the online version of record will be different from this version once it has been copyedited and typeset.
PLEASE CITE THIS ARTICLE AS DOI: 10.1063/5.0107667

References

[1] L. Xu, C.A. Curwen, P.W.C. Hon, Q.-S. Chen, T. Itoh, and B.S. Williams, Appl. Phys. Lett. **107**, 221105 (2015).
[2] L. Xu, C.A. Curwen, D. Chen, J.L. Reno, T. Itoh, and B.S. Williams, IEEE J. Sel. Top. Quantum Electron. **23**, (2017).
[3] C.A. Curwen, J.L. Reno, and B.S. Williams, Appl. Phys. Lett. **113**, 011104 (2018).
[4] C.A. Curwen, J.L. Reno, and B.S. Williams, Nat. Photonics **13**, 855 (2019).
[5] Y. Wu, S. Addamane, J.L. Reno, and B.S. Williams, Appl. Phys. Lett. **119**, 111103 (2021).
[6] L. Xu, D. Chen, T. Itoh, J.L. Reno, and B.S. Williams, Opt. Express **24**, 24117 (2016).
[7] N. Laman and D. Grischkowsky, Appl. Phys. Lett. **93**, 051105 (2008).
[8] Y. Shen, A.D. Kim, M. Shahili, C.A. Curwen, S. Addamane, J.L. Reno, and B.S. Williams, Appl. Phys. Lett. **119**, 181108 (2021).
[9] L. Xu, C.A. Curwen, J.L. Reno, and B.S. Williams, Appl. Phys. Lett. **111**, 101101 (2017).
[10] C.A. Curwen, J.L. Reno, and B.S. Williams, Electron. Lett. **56**, 1264 (2020).
[11] B.S. Williams, S. Kumar, Q. Hu, and J.L. Reno, Opt. Express **13**, 3331 (2005).
[12] A. Barkan, F.K. Tittel, D.M. Mittleman, R. Dengler, P.H. Siegel, G. Scalari, L. Ajili, J. Faist, H.E. Beere, E.H. Linfield, A.G. Davies, and D.A. Ritchie, Opt. Lett. **29**, 575 (2004).
[13] P. Khosropanah, A. Baryshev, W. Zhang, W. Jellema, J.N. Hovenier, J.R. Gao, T.M. Klapwijk, D.G. Paveliev, B.S. Williams, S. Kumar, Q. Hu, J.L. Reno, B. Klein, and J.L. Hesler, Opt. Lett. **34**, 2958 (2009).
[14] D. Rabanus, U.U. Graf, M. Philipp, O. Ricken, J. Stutzki, B. Vowinkel, M.C. Wiedner, C. Walther, M. Fischer, and J. Faist, Opt. Express **17**, 1159 (2009).
[15] Y. Ren, D.J. Hayton, J.N. Hovenier, M. Cui, J.R. Gao, T.M. Klapwijk, S.C. Shi, T.Y. Kao, Q. Hu, and J.L. Reno, Appl. Phys. Lett. **101**, 101111 (2012).
[16] C.A. Curwen, A.D. Kim, Y. Wu, Y. Shen, D.J. Hayton, J.H. Kawamura, B.S. Karasik, S. Addamane, J.L. Reno, and B.S. Williams, Proc. SPIE PC11984, Vertical External Cavity Surface Emitting Lasers (VECSELs) XI, PC1198402 (2022).
[17] S. Barbieri, W. Maineult, S.S. Dhillon, C. Sirtori, J. Alton, N. Breuil, H.E. Beere, and D.A. Ritchie, Appl. Phys. Lett. **91**, 143510 (2007).
[18] A. Mottaghizadeh, D. Gacemi, P. Laffaille, H. Li, M. Amanti, C. Sirtori, G. Santarelli, W. Hänsel, R. Holzwart, L.H. Li, E.H. Linfield, and S. Barbieri, Optica **4**, 168 (2017).
[19] M. Rösch, G. Scalari, M. Beck, and J. Faist, Nat. Photonics **9**, 42 (2014).
[20] A. Forrer, Y. Wang, M. Beck, A. Belyanin, J. Faist, and G. Scalari, Appl. Phys. Lett. **118**, 131112 (2021).
[21] M. Piccardo, B. Schwarz, D. Kazakov, M. Beiser, N. Opačak, Y. Wang, S. Jha, J. Hillbrand, M. Tamagnone, W.T. Chen, A.Y. Zhu, L.L. Columbo, A. Belyanin, and F. Capasso, Nature **582**, 360 (2020).
[22] M. Jaidl, N. Opačak, M.A. Kainz, S. Schönhuber, D. Theiner, B. Limbacher, M. Beiser, M. Giparakis, A.M. Andrews, G. Strasser, B. Schwarz, J. Darmo, and K. Unterrainer, Optica **8**, 780 (2021).
[23] P. Tzenov, I. Babushkin, R. Arkhipov, M. Arkhipov, N. Rosanov, U. Morgner, and C. Jirauschek, New J. Phys. **20**, 053055 (2018).
[24] B. Schneider, F. Kapsalidis, M. Bertrand, M. Singleton, J. Hillbrand, M. Beck, and J. Faist, Laser Photonics Rev. **15**, 2100242 (2021).
[25] G. Wysocki, R.F. Curl, F.K. Tittel, R. Maulini, J.M. Bulliard, and J. Faist, Appl. Phys. B Lasers Opt. **81**, 769 (2005).
[26] I. Galli, M. Siciliani De Cumis, F. Cappelli, S. Bartalini, D. Mazzotti, S. Borri, A. Montori, N. Akikusa, M. Yamanishi, G. Giusfredi, P. Cancio, and P. De Natale, Appl. Phys. Lett. **102**, 121117 (2013).
[27] R.M. Williams, J.F. Kelly, J.S. Hartman, S.W. Sharpe, M.S. Taubman, J.L. Hall, F. Capasso, C. Gmachl, D.L. Sivco, J.N. Baillargeon, and A.Y. Cho, Opt. Lett. **24**, 1844 (1999).
[28] M.S. Taubman, T.L. Myers, B.D. Cannon, R.M. Williams, F. Capasso, C. Gmachl, D.L. Sivco, and A.Y. Cho, Opt. Lett. **27**, 2164 (2002).
[29] S. Bartalini, L. Consolino, P. Cancio, P. De Natale, P. Bartolini, A. Taschin, M. De Pas, H. Beere, D. Ritchie, M.S. Vitiello, and R. Torre, Phys. Rev. X **4**, 021006 (2014).

AIP Publishing

Applied Physics Letters ACCEPTED MANUSCRIPT

This is the author's peer reviewed, accepted manuscript. However, the online version of record will be different from this version once it has been copyedited and typeset.

PLEASE CITE THIS ARTICLE AS DOI: 10.1063/5.0107667

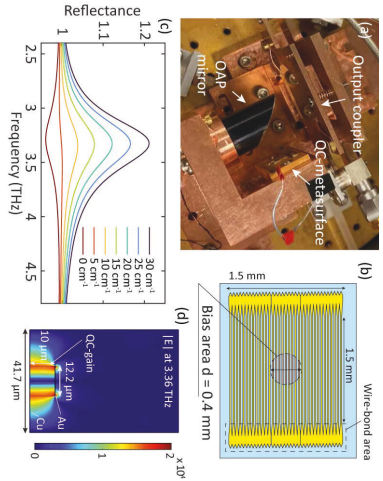

AIP Publishing

Applied Physics Letters ACCEPTED MANUSCRIPT

This is the author's peer reviewed, accepted manuscript. However, the online version of record will be different from this version once it has been copyedited and typeset.

PLEASE CITE THIS ARTICLE AS DOI: 10.1063/5.0107667

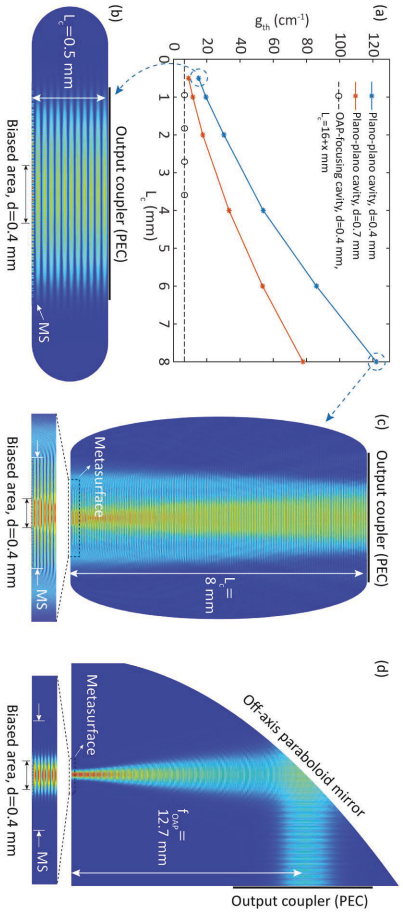

AIP Publishing

Applied Physics Letters

ACCEPTED MANUSCRIPT

This is the author's peer reviewed, accepted manuscript. However, the online version of record will be different from this version once it has been copyedited and typeset.

PLEASE CITE THIS ARTICLE AS DOI: 10.1063/5.0107667

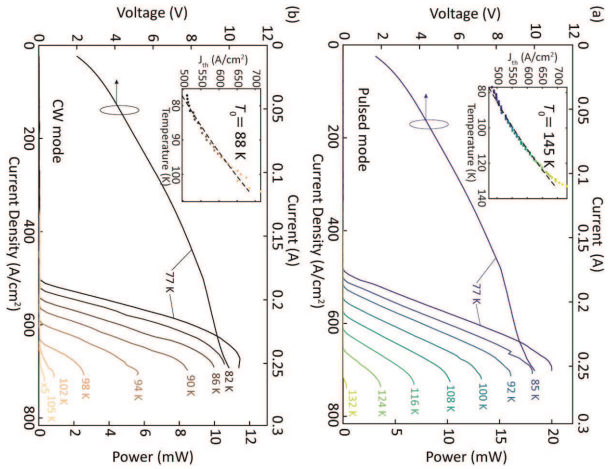

AIP Publishing

Applied Physics Letters ACCEPTED MANUSCRIPT

This is the author's peer reviewed, accepted manuscript. However, the online version of record will be different from this version once it has been copyedited and typeset.

PLEASE CITE THIS ARTICLE AS DOI: 10.1063/5.0107667